RAA 2014 Vol. **14** No. **12**, 1633–1641 doi: 10.1088/1674–4527/14/12/011
http://www.raa-journal.org *http://www.iop.org/journals/raa*

Research in Astronomy and Astrophysics

Performance evaluation of lunar penetrating radar onboard the rover of CE-3 probe based on results from ground experiments *

Hong-Bo Zhang[1], Lei Zheng[1], Yan Su[1], Guang-You Fang[2], Bin Zhou[2], Jian-Qing Feng[1], Shu-Guo Xing[1], Shun Dai[1], Jun-Duo Li[1], Yi-Cai Ji[2], Yun-Ze Gao[2], Yuan Xiao[1], Chun-Lai Li[1]

[1] Key Laboratory of Lunar and Deep Space Exploration, National Astronomical Observatories, Chinese Academy of Sciences, Beijing 100012, China; *zlei@bao.ac.cn*

[2] Institute of Electronics, Chinese Academy of Sciences, Beijing 100190, China

Received 2014 July 23; accepted 2014 September 17

Abstract Lunar Penetrating Radar (LPR) onboard the rover that is part of the Chang'e-3 (CE-3) mission was firstly utilized to obtain in situ measurements about geological structure on the lunar surface and the thickness of the lunar regolith, which are key elements for studying the evolutional history of lunar crust. Because penetration depth and resolution of LPR are related to the scientific objectives of this mission, a series of ground-based experiments using LPR was carried out, and results of the experimental data were obtained in a glacial area located in the northwest region of China. The results show that the penetration depth of the first channel antenna used for LPR is over 79 m with a resolution of 2.8 m, and that for the second channel antenna is over 50.8 m with a resolution of 17.1 cm.

Key words: Moon — techniques: radar astronomy — methods: analytical

1 INTRODUCTION

The subsurface geological structure is of great importance for studying the origin and evolution of lunar crust. Because of the absence of an atmosphere, the subsurface, which is composed of lunar soil and rock fragments, is the boundary layer between the solid part of the Moon and the matter and energy that fill the solar system. Studying the subsurface is important for understanding the earlier evolution of the solar system, properties of the solar wind, composition of the crust and the evolutional history of the Moon as well as acquiring new scientific information (Ouyang 2005).

The internal structure of the Moon has been a topic for discussion and planning since the Apollo program started in the 1960s. The information provided by natural and artificial seismic studies indicates that the Moon can be divided into a crust, mantle and core, a model which is analogous to the Earth. The thickness of the outermost shell is 60$\sim$65 km and the upper 1$\sim$2 km is mainly composed of regolith and rock fragments. Investigation of samples returned by the Apollo missions shows that lunar soil is mainly composed of rock fragments, breccias, glasses and meteorite

* Supported by the National Natural Science Foundation of China.

fragments. A hyperbolic relationship was found between the soil density and depth. The dielectric constant of the soil is 2.3∼3.5 and the loss tangent is 0.005∼0.009. The highlands mainly consist of anorthosites while the maria are mainly composed of basalts that have a dielectric constant of 6.6∼8.6 and a loss tangent of 0.009∼0.016 (Heiken et al. 1991). Observational data acquired by 70 cm ground based radar and the abundance of iron and titanium on the nearside of the Moon have been used by Shkuratov and Bondarenko to produce the first map that shows the distribution of the thickness of regolith. The average depth of lunar soil in maria is 4∼5 m and that in highlands is 10∼15 m (Shkuratov & Bondarenko 2001). Fa & Jin (2010) produced an inverse map of regolith depth for the entire Moon using data taken from a microwave radiometer carried by Chang'e-1 and the ultraviolet-visible spectral data from Clementine. The Lunar Radar Sounder (LRS) onboard the Japanese spacecraft SELENE explored the stratified structure of the subsurface with a detection depth greater than 5 km and a thickness resolution of 75 m (Ono et al. 2008). Some mare areas on the nearside have structure that can be seen in stratigraphy studies; most of the interfaces of the strata lie at a depth of hundreds of meters, with the deepest place currently known being 1050 m (Ono et al. 2009).

The Lunar Penetrating Radar (LPR) onboard the Chang'e-3 (CE-3) rover represents the first time that humans have used ground penetrating radar on the surface of the Moon to detect subsurface geological structure. The scientific goal is to investigate the thickness of the regolith layer as well as the shell structure of the Moon along the route traversed by the rover (Ip et al. 2014). Compared with previous methods of detection, this study concentrates more on gaining information about the shallow layer. The expected detection depth is 100 m with the highest resolution reaching the decimeter scale. The acquired data can reveal more about the origin and evolution of the Moon.

A ground test is an important tool for verifying the potential quality of scientific results obtained with the LPR. From the ground test, we can determine the subsurface detection ability of the LPR, and verify and improve the data processing method. A series of ground tests is carried out. We set up a hierarchical model according to the test results and analyze the depth measurement ability and the thickness resolution.

In Section 2, the properties of the LPR is first introduced. Then in Section 3, the location of the ground experiment is selected. In Section 4, the results and performance of the ground experiment are analyzed. Conclusions are given in Section 5.

2 INSTRUMENT PROPERTIES

The LPR, like the Ground Penetrating Radar (GPR), uses the Ultra Wide Band (UWB) impulse technique, and transmits UWB signals when the the rover, named Yutu, moves along its designated route. Echoes will be produced when the signals encounter interfaces in the medium under the surface of the Moon, and are received and identified by the LPR, which can be used for the detection of subsurface structure (Fang et al. 2014).

The LPR has two detection channels: the first one is designed to detect the structure of lunar shallow crust with one transmitting dipole and one receiving dipole; the center frequency of the transmitted unipolar pulse signal is 60 MHz. The second channel is designed to detect the thicknesses of the lunar regolith with one transmitting bow tie antenna and two receiving bow tie antennas marked A and B respectively. The center frequency of the transmitted bipolar pulse signals is 500 MHz. The main properties of the LPR are listed in Table 1.

In the ground experiment, an LPR prototype is carried by a 1:1 model of the CE-3 lunar rover. In addition, a GPS receiver (device model TRIMBLE R8 GNSS) is attached to trace the path taken by the LPR, as shown in Figure 1. The performance of the LPR prototype is almost the same as the actual one, except the latter is installed with certain isolators and filters to avoid the influence of communication signals between the lunar rover and the lunar lander. The differences between the filtering settings have no notable influences on the results of the ground experiment.

Table 1 Technical Parameters of the LPR Onboard the CE-3 Lunar Rover

Parameter	First channel value	Second channel value
Antenna Type	Dipole	Bow tie
Antenna Center Frequency (MHz)	60	500
Antenna Band (MHz)	41	500
Antenna VSWR	≤ 3	≤ 1.8
Transmitter Pulse Amplitude (V)	1000 (with 5% bias)	400 (with 5% bias)
Transmitter Pulse Repetition Frequency (kHz)	0.5, 1, 2	5, 10, 20
Transmitter Pulse Rising Time (ns)	≤ 2	≤ 1
Receiver Band (MHz)	10.193	10.1359
Receiver Sample Rate (MHz)	400	3200
Receiver Dynamic Range (dB)	103.3	96.7
System Gain (dB)	152	133.3
Standard Data Rate (bps)	6.94K	
Total Mass (kg)	≤ 5.5	
Power (W)	9.8	

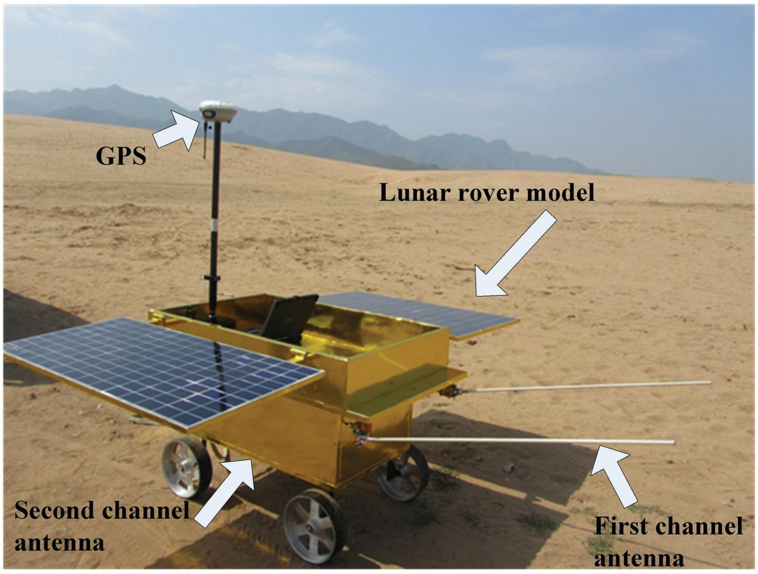

Fig. 1 The LPR prototype onboard a model of the CE-3 lunar rover.

3 GROUND EXPERIMENT

According to the principles governing GPR, the detection capability of LPR is not only related to its technical performance, but also depends on the electromagnetic properties of the lunar subsurface (Dai et al. 2014). Therefore, in order to analyze the depth and thickness resolution of LPR, some places on Earth with similar electromagnetic properties as Mare Imbrium should be selected for the location of the ground experiment.

3.1 Lunar Soil Simulant

The site where the ground experiment is conducted, located in the China Academy of Space Technology, is built according to requirements for the lunar soil simulant, and its electromagnetic

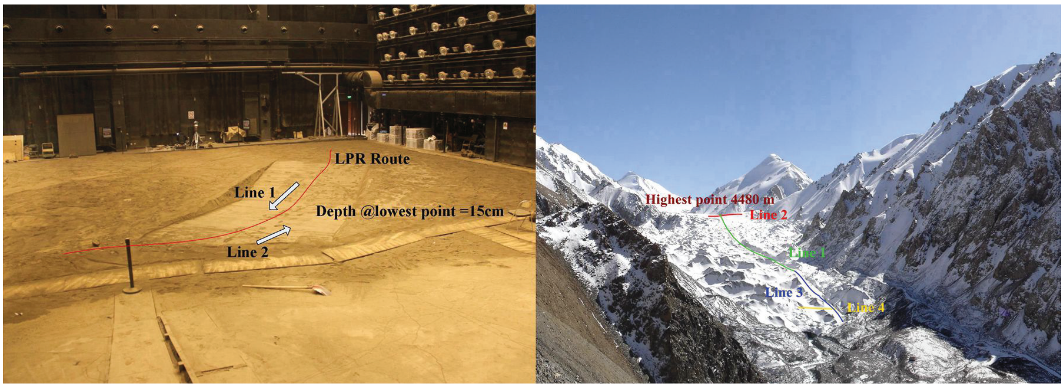

Fig. 2 Site of the ground experiment. *Left*: Site of the artificial lunar regolith experiment. *Right*: Site of the alpine glacier experiment.

characteristics are very close to those of lunar regolith. In the ground experiment, we can verify the validity of the data processing method used for LPR and measure the detection accuracy of the experimental result. We can also derive the minimum resolvable thickness of the second channel in the ground experiment which will approximate the thickness resolution of the lunar regolith. The experiment site is built with a soil layer varying from 15 cm to 70 cm in thickness, and two sets of measurement data are obtained along Lines 1 and 2 (as shown in Fig. 2 (left)).

3.2 Alpine Glacier

According to the detection results obtained from the Apollo program, the subsurface of Mare Imbrium is mainly a basalt structure, and is absolutely dry (Heiken et al. 1991). It is hard to find such areas on Earth. Therefore, we selected an alpine glacial area, which has relatively weak electromagnetic attenuation. The alpine glacier experiment was conducted on the Laohugou Glacier No. 12 in the Qilian Mountains. A photo of the experiment site is shown in Figure 2 (right). The experiment acquired four sets of data along four survey lines, including the areas with the thickest and the thinnest layers of ice: Survey Lines 1 and 3 follow vertical paths in ranges of altitudes of 4400–4480 m and 4434–4354 m, respectively. Survey lines 2 and 4 follow horizontal paths near altitudes 4290 m and 4465 m, respectively.

4 RESULTS AND PERFORMANCE ANALYSIS

4.1 Results

Figure 3 shows the result from the LPR second channel for line 2 in the artificial lunar regolith. From the results of the five tests, the average value of the dielectric constant is 3.2. As can be seen from the figure, these results are consistent with hierarchical structures. In addition, echoes can still be distinguished even in the area that is 0.15 m thick, which means the thickness resolution of the second channel used by the LPR in the simulated lunar regolith is higher than 0.15 m.

Figures 4 and 5 show the maximum penetration depth along the survey lines for the first and second channels obtained by the LPR respectively. As can be seen from Figure 5, the radar signal penetrated the ice layer and reached the bedrock. The maximum penetration depth of the first channel is 152 m, where there is an echo deep down near 91–115 m. Comparing results from the alpine

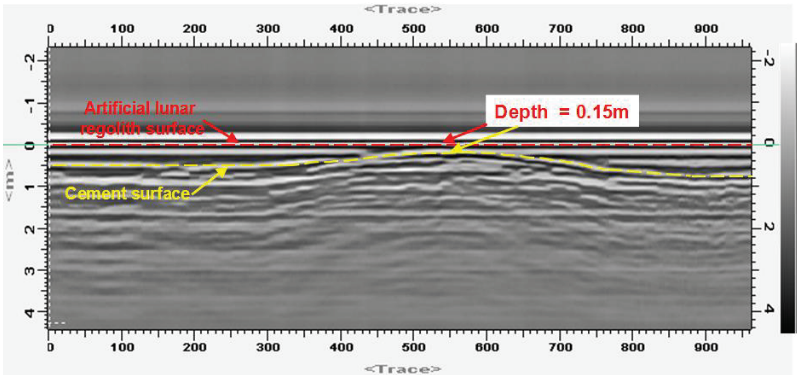

Fig. 3 The result of the LPR second channel in the area with artificial lunar regolith.

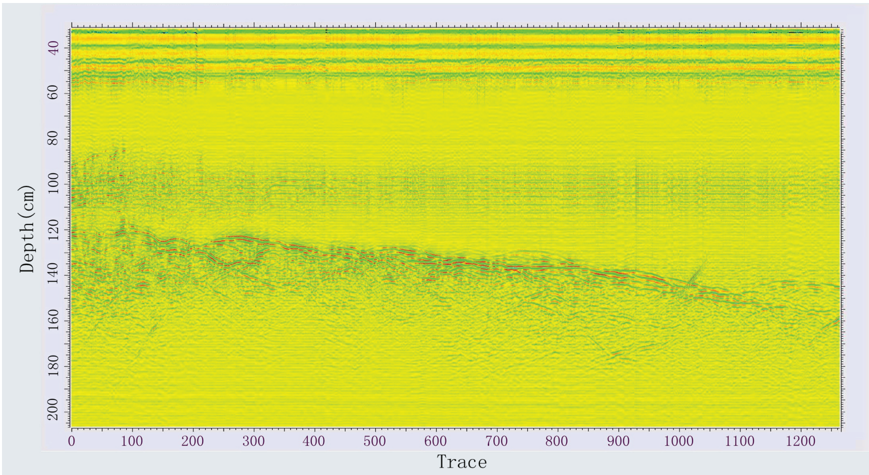

Fig. 4 The results for the maximum penetration depth in the mountain glacial area from the LPR first channel.

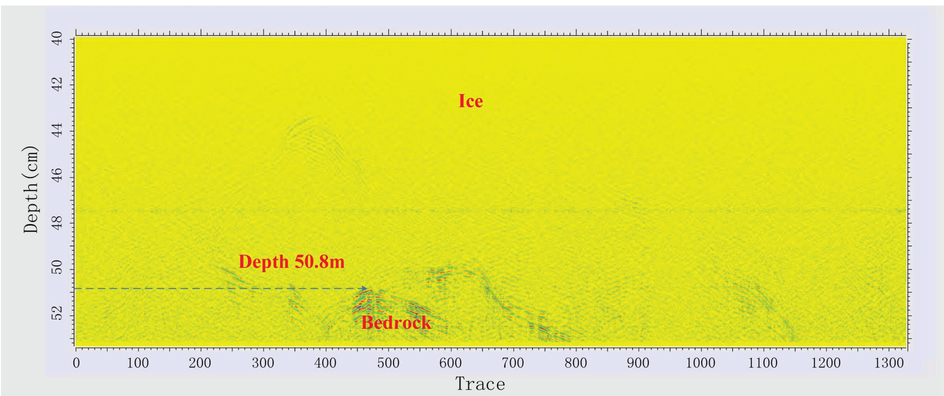

Fig. 5 The results for the maximum penetration depth in the mountain glacial area from the LPR second channel.

Fig. 6 A uniform hierarchical model for the subsurfaces of the Moon and glacier. *Top*: A five-layer model for the glacier subsurface. *Bottom*: A three-ayer model for the lunar subsurface.

glacier experiment (Wu et al. 2009) suggests that there may be an area where ice and rock are mixed together. The maximum penetration depth of the second channel is 50.8 m.

4.2 Performance Analysis

4.2.1 Penetration depth

By calculating the energy loss in the transmission path, the depth detection capability of the LPR can be evaluated. The internal hierarchical structure of the glaciers was modeled according to the LPR experiment on the alpine glaciers, as shown in Figure 6 (top); and the lunar subsurface structure model was established on the basis of early detection results, as shown in Figure 6 (bottom). Analysis with the model assumes that each layer is a homogeneous medium, the radar signal can be modeled as a plane wave and the angle of incidence for each layer is zero.

Considering attenuation that takes place during propagation through a lossy medium, and the transmission and reflection losses at the interfaces between two different media, a wave propagating through a lossy dielectric material in the positive z-direction can be described by (Daniels 2004)

$$E = E_0 e^{-\alpha z}, \tag{1}$$

where E_0 represents the initial amplitude of the radar wave, z represents the propagation distance and the attenuation coefficient, α, may be expressed as

$$\alpha = \omega\sqrt{\mu\varepsilon}\sqrt{\frac{1}{2}\left(\sqrt{1+\tan^2\delta}-1\right)}. \tag{2}$$

Here ω represents the angular frequency of the radar, μ represents the permeability of the medium, ε represents the real part of the dielectric constant of the medium and tan δ represents the dielectric loss tangent.

According to the reflection and transmission properties of a plane wave at the interface of different media, when the incident angle is 0, the reflected and transmission losses of the electric field amplitude can be expressed as (Su et al. 2006)

$$E = \mathrm{E}_0\left|\frac{\eta_1-\eta_2}{\eta_1+\eta_2}\right|, \tag{3}$$

$$E = \mathrm{E}_0\left|\frac{2\eta_2}{\eta_1+\eta_2}\right|, \tag{4}$$

where η_1 and η_2 represent the wave impedance of the incident medium and the transmission medium respectively. These can be expressed as

$$\eta \approx \sqrt{\mu_0/\varepsilon_0\varepsilon}, \tag{5}$$

where μ_0 represents the permeability of a vacuum, and ε_0 and ε represent the real component of the dielectric constant for a vacuum and the given medium.

Therefore, in the alpine glacier experiment, the total loss of the radar wave in the transmission path can be expressed as

$$\begin{aligned} L_{\text{glacier}} &= \frac{4\eta_{\text{ice}}}{(1+\eta_{\text{ice}})^2}\exp\left[-\alpha_{\text{ice}}\left(D_{\text{ice\_1}}+D_{\text{ice\_2}}\right)\right]^2\frac{\eta_{\text{ice}}-\eta_{\text{base\_rock}}}{\eta_{\text{ice}}+\eta_{\text{base\_rock}}} \\ &\quad\times\exp\left(-\alpha_{\text{ice\_rock}}D_{\text{ice\_rock}}\frac{\sqrt{\varepsilon_{\text{ice}}}}{\sqrt{\varepsilon_{\text{ice\_rock}}}}\right)^2\frac{16\eta^2_{\text{ice\_rock}}\eta^2_{\text{ice}}}{(\eta_{\text{ice}}+\eta_{\text{ice\_rock}})^4}, \end{aligned} \tag{6}$$

where $D_{\text{ice\_1}}$, $D_{\text{ice\_1}}$ and $D_{\text{ice\_rock}}$ are the thicknesses of different glacial layers, as shown in Figure 6(top). The lunar subsurface detection capabilities of the LPR first channel with the same attenuation is actually equal to the penetration depth D_{rock}, as shown in Equation (7)

$$\begin{aligned} L_{\text{glacier}} &= \frac{4\eta_{\text{regolith}}}{(1+\eta_{\text{regolith}})^2}\exp\left(-\alpha_{\text{regolith}}d_{\text{regolith}}\right)^2\frac{4\eta_{\text{rock}}\eta_{\text{regolith}}}{(\eta_{\text{regolith}}+\eta_{\text{rock}})^2} \\ &\quad\times\exp\left[-\alpha_{\text{rock}}\left(D_{\text{rock}}-d_{\text{regolith}}\right)\right]^2\frac{\eta_{\text{rock}}-\eta_{\text{next\_layer}}}{\eta_{\text{rock}}+\eta_{\text{next\_layer}}}. \end{aligned} \tag{7}$$

According to Equations (6) and (7), the depth detection ability of the LPR first channel ranges from 79 to 198 m. The parameters of the selected medium are shown in Table 2, in which parameters describing the electromagnetic properties of the ice-rock mixture were taken to be the mean values of ice and bedrock.

Since the LPR second channel only focused on the structure of lunar regolith, we consider its depth detection ability in lunar regolith. According to Table 2, the electromagnetic properties of lunar regolith are very similar to those of the glacier, so the lunar regolith detection ability of the LPR second channel is approximately equal to its ability to detect the depth of the glacier. On the basis of the results obtained by the experiment on the glacier, the lunar regolith detection ability of LPR second channel is higher than 50.8 m.

Table 2 Electromagnetic Parameters of Media Used in This Study

Parameter	Value
Ice $\varepsilon_{\rm ice}$	3.2
Ice $\tan\delta_{\rm ice}$	0.006–0.01
Lunar regolith depth	4–5.2 m
Lunar regolith $\varepsilon_{\rm regolith}$	2.32–3.41
Lunar regolith $\tan\delta_{\rm regolith}$	0.005–0.009
Lunar Mare basalts $\varepsilon_{\rm rock}$	6.62–8.59
Lunar Mare basalts $\tan\delta_{\rm rock}$	0.0093–0.016
Ice bedrock $\varepsilon_{\rm base\_rock}$	5–9
Mixed ice and rocks $\varepsilon_{\rm ice\_rock}$	4.1–6.1
Mixed ice and rocks $\tan\delta_{\rm ice\_rock}$	0.053–0.055
Rock or layer in Mare basalts $\varepsilon_{\rm next\_layer}$	6.6–8.8
$D_{\rm ice\_1}$	91
$D_{\rm ice\_2}$	37
$D_{\rm ice\_rock}$	24

4.2.2 Depth resolution

According to the principle governing ground penetrating radar, the depth resolution T of the LPR is inversely proportional to the dielectric constant of the lunar subsurface, as shown in Equation (8)

$$T = \frac{c}{2B\sqrt{\varepsilon}}\,, \tag{8}$$

where c represents the speed of light, B denotes the effective bandwidth of the radar signal, and ε is the real part of the dielectric constant of the medium. Therefore, the depth resolution of the lunar subsurface can be calculated based on the minimum depth resolution obtained by the LPR ground experiment, as shown in Equation (9).

$$T_{\rm lunar\_subsurface} = T_{\rm ground\_experiment} \times \frac{\sqrt{\varepsilon_{\rm ground\_experiment}}}{\sqrt{\varepsilon_{\rm lunar\_subsurface}}}\,, \tag{9}$$

where $T_{\rm lunar\_subsurface}$ and $T_{\rm ground\_experiment}$ denote the depth resolutions for the lunar subsurface and the ground tests respectively; $\varepsilon_{\rm lunar\_subsurface}$ and $\varepsilon_{\rm ground\_experiment}$ represent the real part of the dielectric constant for the lunar subsurface and the tested medium, respectively.

The minimum thickness measured in the glacier with the LPR first channel is 4 m. Then according to Equation (9), the depth resolution of the LPR first channel in mare basalt is higher than 2.8 m. Similarly, the depth resolution of the LPR second channel in lunar regolith is better than 17.1 cm.

5 CONCLUSIONS

The characteristics of LPR as well as tests performed on the lunar soil simulant and a dry land glacier are introduced in this paper. The test results of the lunar soil simulant show that the detection results are consistent with a layered structure that has been incorporated in the model, which indicates that the data processing method for LPR is correct and the measured depth values are accurate. We establish a uniform layered model according to test results from a dry land glacial area and analyze the detection ability of LPR in the subsurface by calculating the total loss of a radar wave in the path of propagation. The results show the first channel's depth detection ability for LPR is better than 79 m; and the second one is better than 50.8 m. At the same time, the thickness resolution of the LPR in the subsurface is evaluated by the minimum layered thickness in the lunar soil simulant and glacier, which shows the thickness resolution of the first channel in the mare basalts is better than 2.8 m, and the second one is better than 17.1 cm.

However, there are still some problems that can affect the final results. First of all, the detection depth is calculated by the dielectric constant of the surface without considering changes with the depth. Secondly, the uniform hierarchical model is inconsistent with the actual situation. Due to conditions of the experiment, we could not acquire an ice core from the detection area, so the accuracy of the glacial stratigraphy model cannot be verified. In addition, the second channel did not yield information about stratigraphy that is sufficiently accurate during the glacier test, which affects the ability to distinguish depths calculated from the test results. In fact, the effective bandwidth of the radar wave would be narrowed with depth, which results in a decreasing depth resolution. Thus, the thickness resolution for a depth of 15 cm is only a reference, which does not necessarily represent the most accurate thickness resolution of the second channel.

Acknowledgements This work was supported by the National Natural Science Foundation of China (Grant No. 11203046).

References

Dai, S., Su, Y., Xiao, Y., et al. 2014, RAA (Research in Astronomy and Astrophysics), 14, 1642
Daniels, D. 2004, Ground Penetrating Radar (2nd edn.; London: The Institution of Electrical Engineers)
Fa, W.-Z., & Jin, Y.-Q. 2010, Scientia Sinica Informations, 40, 115 (in Chinese)
Fang, G.-Y., Zhou, B., Ji, Y.-C., et al. 2014, RAA (Research in Astronomy and Astrophysics), 14, 1607
Heiken, G. H., Vaniman, D. T., & French, B. M. 1991, Lunar Sourcebook - A User's Guide to the Moon (New York: Cambridge Univ. Press)
Ip, W.-H., Yan, J., Li, C.-L., & Ouyang, Z.-Y., 2014, RAA (Research in Astronomy and Astrophysics), 14, 1511
Ono, T., Kumamoto, A., Yamaguchi, Y., et al. 2008, Earth, Planets, and Space, 60, 321
Ono, T., Kumamoto, A., Nakagawa, H., et al. 2009, Science, 323, 909
Ouyang, Z.-Y. 2005, Introduction to Lunar Science (Beijing: China Aerospace Press, in Chinese)
Shkuratov, Y. G., & Bondarenko, N. V. 2001, Icarus, 149, 329
Su, Y., Huang, C.-L., & Lei, W.-T. 2006, Ground Penetrating Radar (GPR) Theory and Application (Beijing: Science Press, in Chinese)
Wu, Z., Liu, S.-Y., & Zhang, S.-Q. 2009, Advances in Earth Science, 24, 149 (in Chinese)